Naval Research Laboratory
Washington, DC 20375-5320

U.S. NAVAL RESEARCH LABORATORY

NRL/6850/MR—2022/2

Epitaxial Integration of Perovskite Oxides with Scandium Aluminum Nitride

ERIC N. JIN

Electromagnetics Technology Branch
Electronics Science and Technology Division

November 21, 2022

DISTRIBUTION STATEMENT A: Approved for public release; distribution is unlimited.

REPORT DOCUMENTATION PAGE

Form Approved
OMB No. 0704-0188

Public reporting burden for this collection of information is estimated to average 1 hour per response, including the time for reviewing instructions, searching existing data sources, gathering and maintaining the data needed, and completing and reviewing this collection of information. Send comments regarding this burden estimate or any other aspect of this collection of information, including suggestions for reducing this burden to Department of Defense, Washington Headquarters Services, Directorate for Information Operations and Reports (0704-0188), 1215 Jefferson Davis Highway, Suite 1204, Arlington, VA 22202-4302. Respondents should be aware that notwithstanding any other provision of law, no person shall be subject to any penalty for failing to comply with a collection of information if it does not display a currently valid OMB control number. **PLEASE DO NOT RETURN YOUR FORM TO THE ABOVE ADDRESS.**

1. REPORT DATE *(DD-MM-YYYY)*
21-11-2022

2. REPORT TYPE
NRL Memorandum Report

3. DATES COVERED *(From - To)*
30-08-2021 – 29-08-2022

4. TITLE AND SUBTITLE
Epitaxial Integration of Perovskite Oxides with Scandium Aluminum Nitride

5a. CONTRACT NUMBER

5b. GRANT NUMBER

5c. PROGRAM ELEMENT NUMBER
NISE

6. AUTHOR(S)
Eric N Jin

5d. PROJECT NUMBER

5e. TASK NUMBER

5f. WORK UNIT NUMBER
N20T

7. PERFORMING ORGANIZATION NAME(S) AND ADDRESS(ES)
Naval Research Laboratory
4555 Overlook Avenue, SW
Washington, DC 20375-5320

8. PERFORMING ORGANIZATION REPORT NUMBER
NRL/6850/MR--2022/2

9. SPONSORING / MONITORING AGENCY NAME(S) AND ADDRESS(ES)
Naval Research Laboratory
4555 Overlook Avenue, SW
Washington, DC 20375-5320

10. SPONSOR / MONITOR'S ACRONYM(S)
NRL/NISE

11. SPONSOR / MONITOR'S REPORT NUMBER(S)

12. DISTRIBUTION / AVAILABILITY STATEMENT
DISTRIBUTION STATEMENT A: Approved for public release; distribution is unlimited.

13. SUPPLEMENTARY NOTES
Karles Fellowship

14. ABSTRACT
This report presents research conducted by Dr. Eric Jin (Code 6852) during his Jerome and Isabella Karle Distinguished Scholar Fellowship from August 30, 2021 – August 29, 2022. It describes the epitaxial growth of thin film functional oxide SrCaTiO3 onto ScAlN high-electron-mobility transistor heterostructures. Structure-property relationships are investigated and the fabrication processes are optimized to maximize the resulting electrical performance of the heterostructures. This new combined materials system demonstrates heterogeneous integration of two very different material classes and paves the way for the development of novel and agile RF and power electronic components serving the needs of the Navy and Department of Defense.

15. SUBJECT TERMS

16. SECURITY CLASSIFICATION OF:			17. LIMITATION OF ABSTRACT	18. NUMBER OF PAGES	19a. NAME OF RESPONSIBLE PERSON
a. REPORT	**b. ABSTRACT**	**c. THIS PAGE**			Eric N. Jin
U	U	U	U	13	**19b. TELEPHONE NUMBER** *(include area code)* (202) 767-3008

Standard Form 298 (Rev. 8-98)
Prescribed by ANSI Std. Z39.18

This page intentionally left blank.

CONTENTS

1. INTRODUCTION 1
2. RESEARCH APPROACH 2
   - 2.1 Plasma-Assisted Molecular Beam Epitaxy 2
   - 2.2 Structural Characterization Techniques 2
   - 2.3 Electrical Characterization Techniques 2
3. EXPERIMENTS 3
   - 3.1 Epitaxial Growth of $Sr_{1-x}Ca_xTiO_3$/ScAlN 3
   - 3.2 Surface Treatment Study of $SrTiO_3$/ScAlN 5
   - 3.3 Modification of TiO_2 Buffer Layer 6
4. CONCLUSIONS 8
5. ACKNOWLEDGEMENTS 8

This page intentionally left blank.

EXECUTIVE SUMMARY

This report presents research conducted by Dr. Eric Jin (Code 6852) during his Jerome and Isabella Karle Distinguished Scholar Fellowship from August 30, 2021 – August 29, 2022. It describes the epitaxial growth of thin film functional oxide $SrCaTiO_3$ onto ScAlN high-electron-mobility transistor heterostructures. Structure-property relationships are investigated and the fabrication processes are optimized to maximize the resulting electrical performance of the heterostructures. This new combined materials system demonstrates heterogeneous integration of two very different material classes and paves the way for the development of novel and agile RF and power electronic components serving the needs of the Navy and Department of Defense.

This page intentionally left blank.

EPITAXIAL INTEGRATION OF PEROVSKITE OXIDES WITH SCANDIUM ALUMINUM NITRIDE

1. INTRODUCTION

The Naval Research and Development Framework prioritizes the development of advanced radio frequency (RF) electronics and materials to establish and maintain spectrum superiority against adversaries. Navy needs for improved RF power amplifiers, RF signal processing devices, and power electronics has provided the motivation to research new materials systems based on ultra-wide bandgap (UWBG; bandgap E_g > 3.4 eV) semiconductors, which can overcome limitations being reached in conventional wide bandgap materials such as gallium nitride (GaN) and silicon carbide (SiC). One emergent material is scandium aluminum nitride ($Sc_xAl_{1-x}N$), an UWBG semiconductor that has recently attracted significant attention due to its 5× higher piezoresponse compared to aluminum nitride (AlN) [1], and has demonstrated ferroelectric polarization switching [2]. These properties make ScAlN an appealing material for wideband filters and ferroelectric memory applications, respectively. NRL was the first to demonstrate epitaxial ScAlN thin films using RF plasma-assisted molecular beam epitaxy (MBE) [3]; this research builds on the technology developed on this epitaxial UWBG semiconductor platform.

Perovskite oxides (chemical formula ABO_3) have been highly studied due to their functional properties that are not observed in conventional semiconductors. Materials such as strontium titanate ($SrTiO_3$ or STO) and strontium calcium titanate ($Sr_{1-x}Ca_xTiO_3$ or SCTO) are examples of oxides that have extremely high dielectric constants (κ > 100), but also support rich phase diagrams that include superconductivity, antiferroelectricity, and ferroelectricity [4]. Integrating these functionalities onto a UWBG semiconductor platform would both improve electric field management in high-electron-mobility transistors (HEMTs) [5] and could lead to new classes of devices based on a hybrid materials platform. Figure 1 shows a schematic of how an epitaxial functional oxide and UWBG semiconductor are combined to form the heterostructures described in this work.

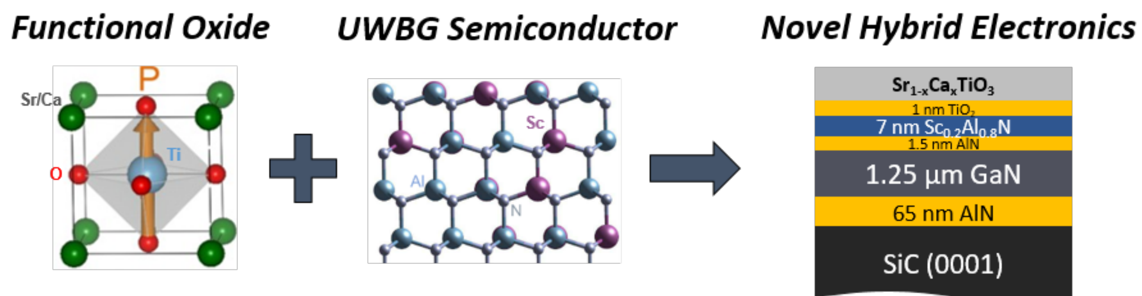

Fig. 1 — Schematic showing the overview of the project, integrating the perovskite oxide $SrCaTiO_3$ (left) with UWBG semiconductor ScAlN (center) to form an epitaxial HEMT heterostructures (right). Many perovskite oxides exhibit unique functionality, including spontaneous polarization (orange labeled "P"), which can lead to ferroelectric behavior.

Manuscript approved October 19, 2022.

The main research accomplishment from this work is the demonstration of a novel hybrid heterostructure comprised of thin film SCTO layers epitaxially grown on ScAlN, and related structural and electrical characterization to support its role as a new functional material to support future DoD electronics. The efforts of this work leveraged results from an ongoing NRL 6.1 base program investigating antiferroelectric materials, directly motivated a new 6.1 base program extending the research of this work, and resulted in two conference presentations and a journal manuscript in preparation.

2. RESEARCH APPROACH

This project utilizes advanced thin film deposition techniques combined with a diverse characterization suite to analyze the materials properties of the fabricated samples.

2.1 Plasma-Assisted Molecular Beam Epitaxy

The heterostructure stacks studied in this work were grown by RF-plasma-assisted nitride and oxide molecular beam epitaxy (MBE). The ScAlN/GaN HEMT structure was first grown using a ScientaOmicron PRO-100 MBE system equipped with dual filament aluminum and high temperature scandium effusion cells. A 65 nm AlN nucleation layer was first grown on a 3-in. 6H-SiC substrate, followed by a 1.25 µm GaN buffer layer, a 1.5 nm AlN interlayer, and finally, a 7 nm thick $Sc_{0.20}Al_{0.80}N$ barrier layer. Further growth details can be found in an earlier publication [8]. The barrier layer thickness was chosen to tune the electron density of the two-dimensional electron gas (2DEG) formed at the ScAlN/GaN interface.

After ScAlN growth, the 3-in. wafer was diced into 10 × 10 mm^2 squares with a diamond saw. These smaller squares were used as substrates for the subsequent STO and SCTO growths. Following previously published work establishing the growth of SCTO on GaN [6] and AlGaN [7], these squares were degreased with solvents and cleaned in a piranha solution (1:5 H_2O_2:H_2SO_4) for 10 minutes at 80 °C before loading into a VG V80H MBE chamber for oxide growth. To minimize the lattice and structural mismatch between wurtzite ScAlN and perovskite STO, a 1 nm TiO_2 buffer layer was deposited at 500 °C using an RF oxygen plasma at 250 W and a gas flow of 0.20 sccm, before the STO and SCTO layers were deposited. The sample stack is summarized in the right schematic of Fig. 1.

2.2 Structural Characterization Techniques

Sample quality was evaluated with both *in situ* and *ex situ* characterization techniques. During MBE growth, real-time sample surface quality was investigated using reflection high-energy electron diffraction (RHEED). Post-growth, morphology was studied using atomic force microscopy (AFM), and crystal structure was studied using x-ray diffraction (XRD) and transmission electron microscopy (TEM).

2.3 Electrical Characterization Techniques

To compare the electrical performance of the HEMT structures, measurements were conducted before and after the oxide deposition. Contactless sheet resistance measurements were performed with a Lehighton tool and Hall effect measurements were performed on samples in a van der Pauw geometry in a permanent magnet (B = 2030 Gauss) Hall station, using indium contacts soldered on the corners. The corners of the samples were scored with a diamond scribe prior to soldering to promote good vertical electrical contact.

3. EXPERIMENTS

3.1 Epitaxial Growth of $Sr_{1-x}Ca_xTiO_3$/ScAlN

A SCTO sample series with varying Ca composition ranging from $x = 0$ (i.e., STO) to $x = 0.38$ was grown on the ScAlN HEMT structure by co-evaporating strontium (Sr), calcium (Ca), and titanium (Ti) source charges from effusion cells in an RF oxygen plasma. The growth rates were calibrated *in situ* with a quartz crystal microbalance and confirmed *ex situ* with x-ray reflectivity measurements. The stoichiometry of the films was studied with x-ray photoemission spectroscopy and calibrated with Rutherford backscattering analysis (not shown). Figure 2 shows structural characterization of this sample set, including RHEED, AFM, and XRD. The SCTO samples grow along the (111) orientation, as is expected based on previous heteroepitaxy studies. The STO (i.e., $x = 0$) sample has the highest crystalline quality, as evidenced by its brightest and spottiest RHEED pattern, and is comparable to the RHEED patterns observed when STO is grown on GaN and AlGaN (Refs. [6] and [7]). However, as the Ca fraction increases, the RHEED patterns indicate a degradation in crystallinity, with the streak intensities becoming more diffuse and patterns exhibiting signs of polycrystallinity (arc features). Furthermore, XRD of the sample series confirms this trend; the XRD intensity of the SCTO peak falls with increasing Ca fraction. AFM performed on the samples indicate rough films with root-mean-square roughness values typically >2 nm.

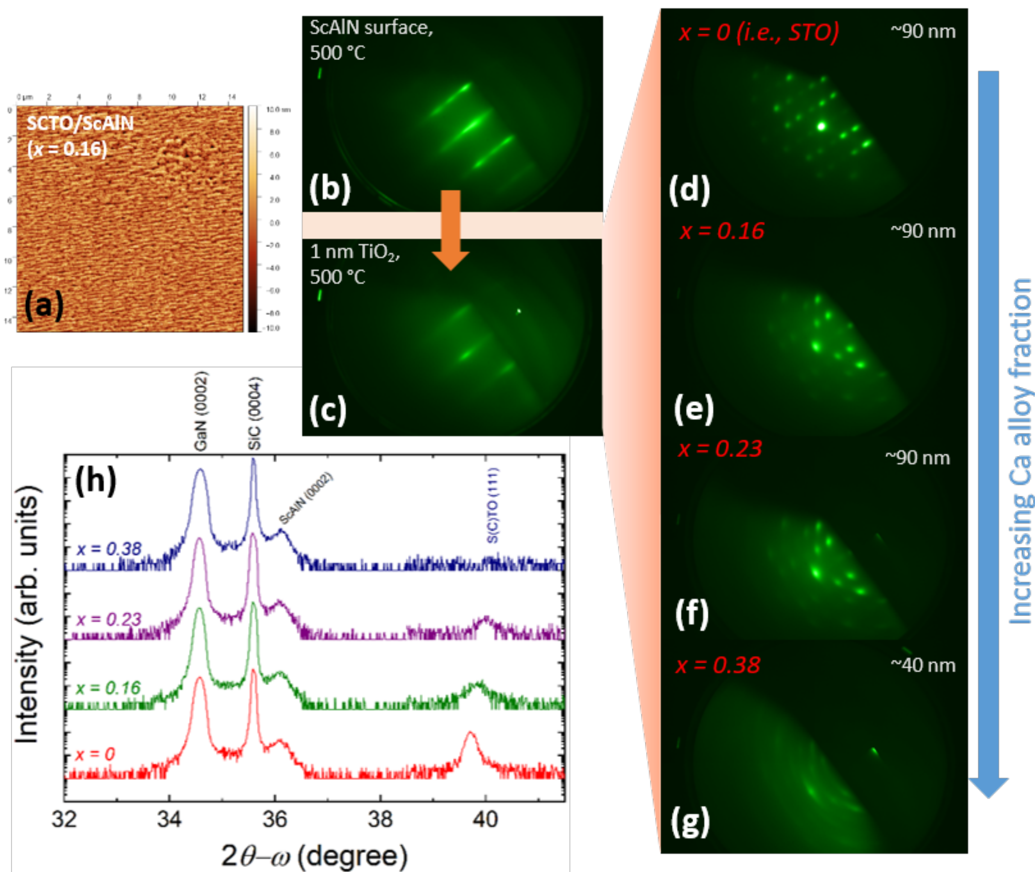

Fig. 2 — Structural characterization of $Sr_{1-x}Ca_xTiO_3$ films grown on ScAlN/GaN/SiC heterostructures. (a) Representative 15×15 μm^2 AFM image of a $Sr_{0.84}Ca_{0.16}TiO_3$ sample surface, with a root-mean-square roughness value of 2.56 nm. RHEED patterns of (b) the starting ScAlN surface after *ex situ* piranha cleaning and prior to oxide layer deposition, (c) 1 nm TiO_2 layer deposited at 500 °C, followed by $Sr_{1-x}Ca_xTiO_3$ layers grown at 650 °C at various compositions: (d) $SrTiO_3$, (e) $Sr_{0.84}Ca_{0.16}TiO_3$, (f)

$Sr_{0.77}Ca_{0.23}TiO_3$, and (g) $Sr_{0.62}Ca_{0.38}TiO_3$. The $x = 0.38$ sample growth was aborted at ~40 nm SCTO thickness due to poor layer crystallinity. (h) XRD linescans comparing the samples in the composition study.

The STO film is expected to grow similarly on ScAlN as on AlGaN, due to their similar lattice constants. Furthermore, the choice in scandium composition of 20% allows the ScAlN film to be nearly lattice-matched to GaN [3], allowing for a similar comparison with STO growth on GaN. The resultant quality of the STO film is similar, as observed both in the RHEED (Fig. 2d) and XRD data (Fig. 2h). However, the electrical properties of the HEMT heterostructure degrade when the STO layers are grown (Table 1). Furthermore, the film becomes less crystalline as more Ca is introduced into the oxide. This points to a possible chemical reaction occurring either between the scandium in the ScAlN and the SCTO film, or on the surface of the ScAlN from the sample pretreatment that inhibits crystallinity during oxide growth. To investigate these effects, TEM imaging and electron energy loss spectroscopy (EELS) were performed on the STO/ScAlN samples (Fig. 3).

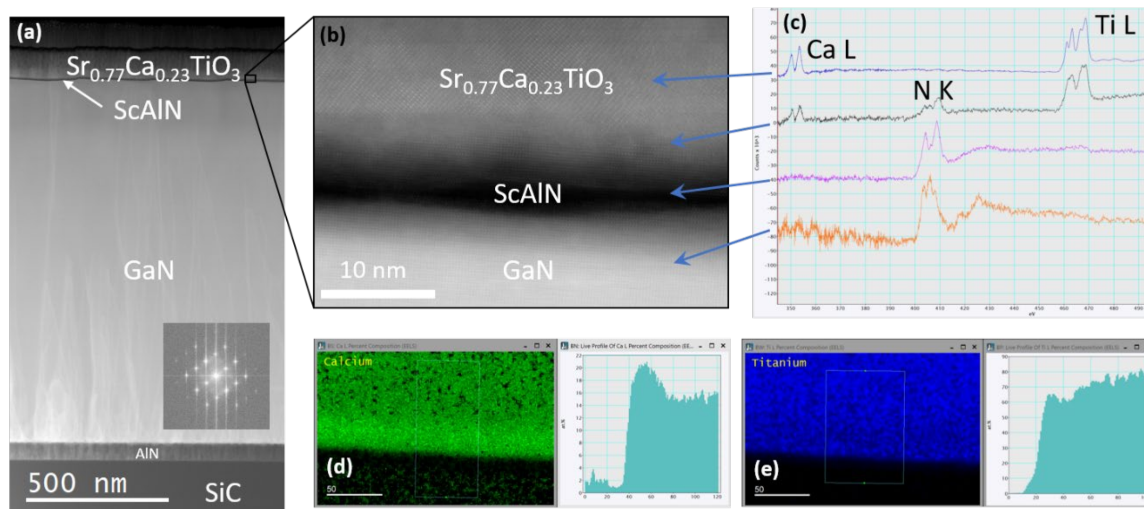

Fig. 3 — TEM imaging and electron energy loss spectroscopy (EELS) performed on a $Sr_{0.77}Ca_{0.23}TiO_3$/ScAlN heterostructure. (a) High angle annular dark field scanning TEM image of the heterostructure stack. Inset shows fast Fourier transform of the SCTO film along the [110] direction. (b) High resolution scanning TEM image at the SCTO/ScAlN/GaN interface. (c) EELS spectra for the Ca *L*, Ti *L,* and N *K* edges from selected points throughout the heterostructure. EELS spectra focusing on calcium (d) and titanium (e), with respective intensities (right) across the SCTO/ScAlN interface, plotted upward (from substrate to oxide layers).

The TEM images confirm the epitaxial relationship between the SCTO and the ScAlN as (111) [11-2] SCTO || (0001) [10-10] GaN, or equivalently, (111) [1-10] SCTO || (0001) [11-20] GaN. The SCTO layers exhibit various grain orientations, all oriented along (111), but rotated with respect to one another. This occurs due to the high strain at the interface, the effects of which are observed in the rough and poorly defined interface between the SCTO layers and the ScAlN, and between the ScAlN and the GaN (Fig 3b). The presence of a degraded interface is consistent with the structural characterization of the SCTO films (Fig. 2) and the degraded electrical characteristics of the HEMT structures with the oxide deposited on top. EELS spectra indicate intermixing at the SCTO-ScAlN interface (Fig. 3c), with nitrogen observed in the first few layers of the SCTO. Furthermore, intensity linescans across the interface also indicate a higher fraction of Ca in the first few layers (right panel of Fig. 3d), providing additional support of a chemical reaction occurring at the SCTO/ScAlN interface.

To determine whether the piranha treatment performed on the ScAlN surface contributed to the degraded interfaces, a surface pre-treatment study was conducted, whereby the ScAlN was prepared with different chemical treatments prior to loading into the MBE system for oxide deposition.

3.2 Surface Treatment Study of $SrTiO_3$/ScAlN

The piranha clean used to prepare the nitride semiconductor substrate before oxide film growth has been previously demonstrated to yield clean surfaces specifically for GaN [9]. However, the ScAlN surface is chemically different from that of GaN, so other methods of surface preparation should be considered to maximize the surface quality prior to oxide deposition. A surface treatment study was performed, where STO was grown on ScAlN prepared with four different surface treatments: 1) phosphoric acid clean (10 minutes at room temperature in 1:3 H_2SO_4:H_3PO_4, based off of a receipt from Ref. [10]), 2) standard piranha clean (10 minutes at 80 °C in 1:5 H_2O_2:H_2SO_4), 3) ultraviolet ozone (O_3) exposure for 10 minutes at room temperature followed by a dilute 30 second hydrofluoric acid dip (1:10 HF:H_2O), and 4) solvent degreasing with acetone and isopropyl alcohol. Following the respective treatments, 40 nm of STO were grown on the ScAlN samples, and Hall measurements were performed to compare the sheet resistance (R_s), electron mobility (μ), and electron density (n_s). The results are shown in Table I. Structural data collected on the samples are shown in Fig. 4.

Table 1 —Electrical Characterization of STO/ScAlN Heterostructures with Varying Surface Preparation

Sample Description	Lehighton R_s (Ω/□)	Hall R_s (Ω/□)	Hall μ ($cm^2V^{-1}s^{-1}$)	Hall n_s ($\times10^{13}$ cm^{-2})
As-grown ScAlN HEMT (no STO)	251	264	796	2.97
Phosphoric acid clean	363	381	487	3.36
Piranha clean	566	695	318	2.82
UV O_3 and HF dip	706	*	*	*
Solvent degrease only	340	382	514	3.18

*Sample had poor electrical contact and Hall effect measurements were inconclusive.

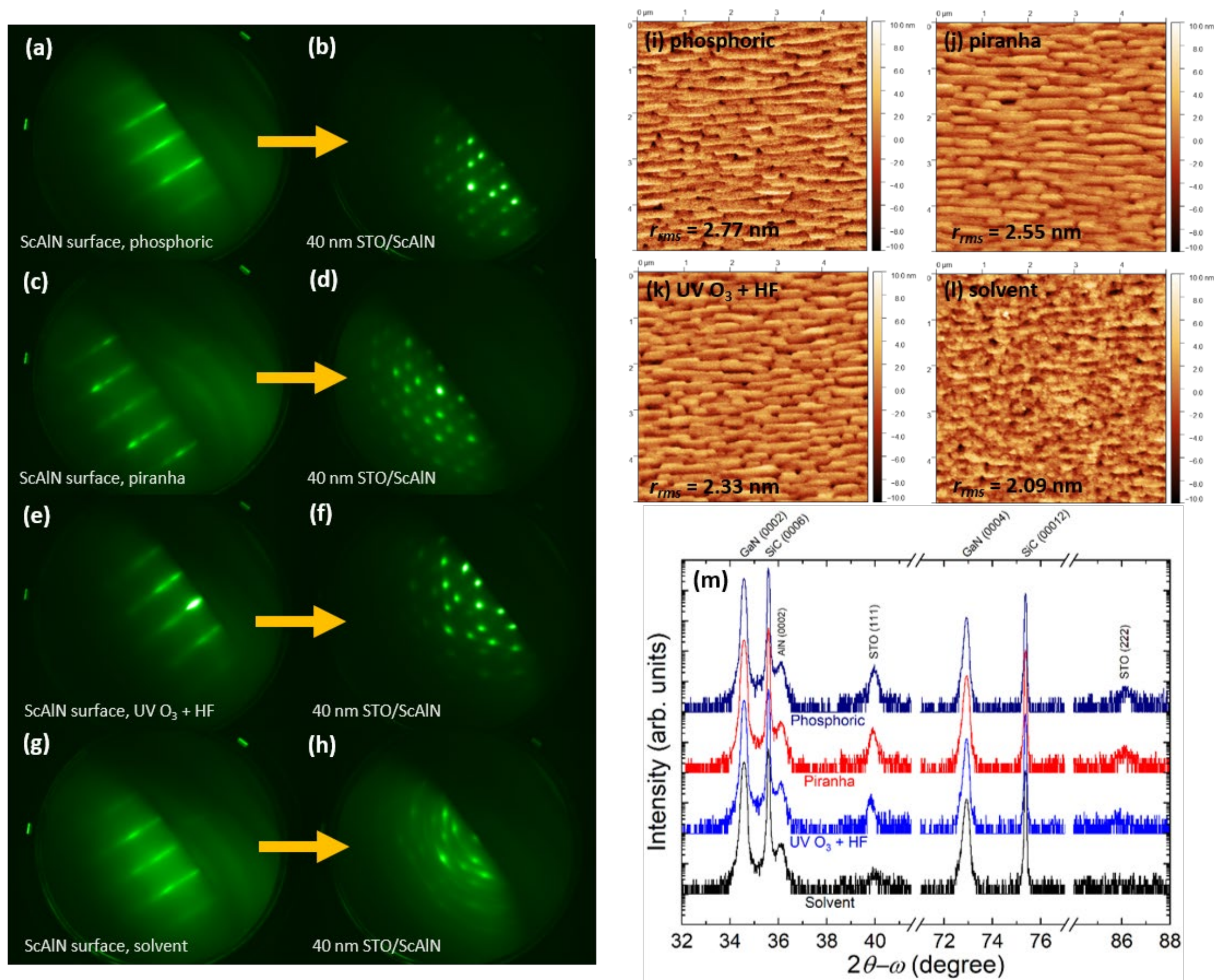

Fig. 4 — Structural characterization of 40 nm STO/ScAlN heterostructures with various chemical treatments prior to oxide layer deposition. Respective RHEED patterns of ScAlN and STO surfaces (a-b) after phosphoric acid clean, (c-d) after piranha clean, (e-f) after UV ozone and HF clean, and (g-h) after solvent clean. (i-l) 5×5 μm^2 AFM images of STO/ScAlN surfaces with respective pre-treatments labeled. Root-mean-square roughness values are listed. (m) XRD 2θ–ω spectra of the four samples studied.

All samples exhibit an increase in R_s and reduction in μ compared to the as-grown ScAlN sample. The solvent degrease and phosphoric acid clean result in an STO film with the least amount of degradation. However, RHEED on the solvent cleaned sample (Figs. 4g and 4h) indicates a polycrystalline STO film and a subsequent change in surface morphology (Fig. 4j), compared to the other samples. The solvent cleaned sample also has the lowest crystallinity by XRD (Fig. 4m). On the other hand, the phosphoric acid cleaned sample exhibits the best structural characteristics. In conclusion, preparation of the ScAlN surface with a phosphoric acid clean leads to the highest quality epitaxial STO and minimizes the reduction in electrical performance.

3.3 Modification of TiO_2 Buffer Layer

Finally, the optimization of the TiO_2 buffer layer was explored, to further maximize electrical properties of the STO/ScAlN HEMT heterostructure. While previous work determined that a 1 nm thick TiO_2 buffer layer resulted in the highest quality of STO and SCTO films grown on GaN [6-7], that specific

recipe is not guaranteed to produce the highest quality films grown on ScAlN, a chemically different semiconductor compared to GaN. As shown in Section 3.2, even a difference in substrate cleaning can lead to very different properties of an epitaxially grown oxide film. Therefore, the first layers grown on the ScAlN surface can be critical in controlling the crystal quality of the subsequent layers.

A study was performed to determine the effects the TiO_2 layer thickness has on the properties of the STO/ScAlN heterostructures prepared with the phosphoric acid clean. Four layer thicknesses of TiO_2 were explored: 1 nm, 2 nm, 5 nm, and 10 nm. Following the TiO_2 deposition, 40 nm of STO were grown on top. The results are summarized in Table 2 and Fig. 5. The variation of TiO_2 layer thickness does not appreciably change the XRD spectra (Fig. 5a), although rocking curves of the STO (111) peak (Fig. 5b) indicate that the sample with the 2 nm TiO_2 layer has the narrowest rocking curve full width at half max (FWHM) value of 0.97°. All the samples grown in this series exhibit higher crystallinity (lower FWHM values) than the piranha treated samples. Electrical characterization of these samples are summarized in Table 2. The sheet resistance of the 10 nm TiO_2 sample is lowest in the series, but the mobility of the original 1 nm sample is the highest, although not by a significant amount. Again, all the phosphoric acid treated samples have lower sheet resistance values and higher electron mobility values than the piranha treated samples. Furthermore, the carrier density of the piranha treated sample is lower as well, indicating that the degraded sample crystallinity reduces the 2DEG density, likely due to additional scattering mechanisms at the interface.

Table 2 — Characterization of STO/ScAlN Heterostructures with Varying TiO_2 Buffer Layers

TiO_2 layer thickness (nm)	**Lehighton R_s (Ω/□)**	**Hall R_s (Ω/□)**	**Hall μ ($cm^2V^{-1}s^{-1}$)**	**Hall n_s ($\times 10^{13}$ cm^{-2})**	**STO (111) XRD rc FWHM**
1 (piranha)	566	695	318	2.82	2.20
1	363	381	487	3.36	1.65
2	436	501	368	3.39	0.97
5	379	377	422	3.92	1.34
10	308	369	468	3.61	1.49

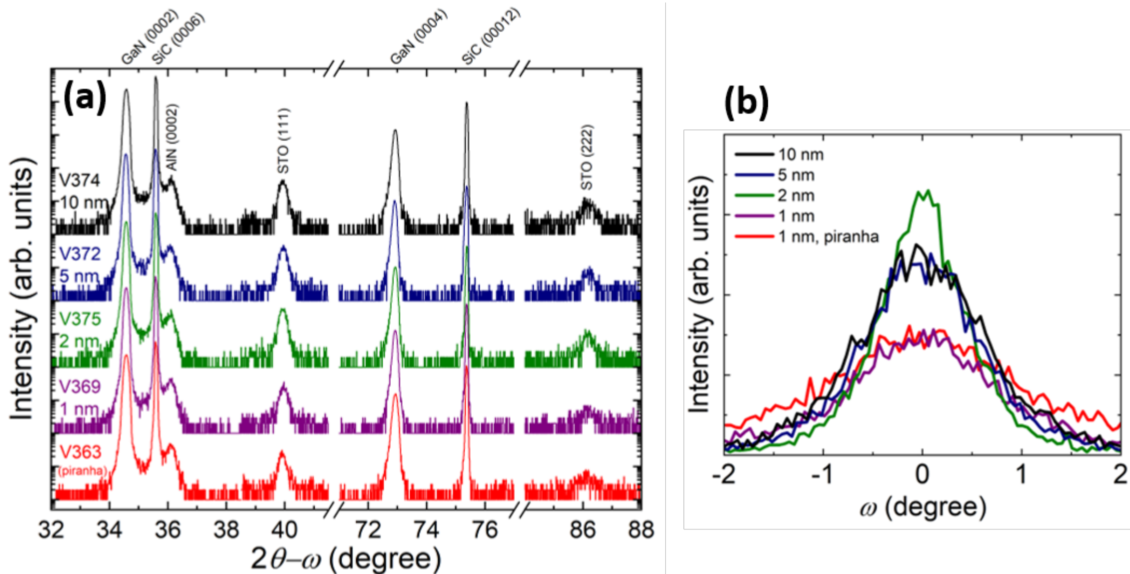

Fig. 5 — XRD characterization of 40 nm STO/ScAlN heterostructures with modified TiO_2 buffer layer thicknesses, all with a phosphoric acid pre-treatment. (a) 2θ–ω spectra. Sample with a 1 nm TiO_2 buffer layer with piranha treatment is shown for comparison. (b) STO (111) rocking curve (rc) comparison.

Because of the mixed structural and electrical characterization results, it is concluded that the thickness of the TiO_2 buffer layer does not significantly affect the properties of STO/ScAlN HEMT heterostructures. These results rule out any potential intermixing between the STO layer and the ScAlN layer as a mechanism for degrading electron mobility, as a thicker TiO_2 layer would increase the spatial separation (and therefore reduce intermixing) between the two layers. The surface preparation of the ScAlN film prior to STO growth is shown to have a far greater impact on controlling the crystallinity of the STO, along with minimizing any degradation to the 2DEG layer in the ScAlN HEMT.

4. CONCLUSIONS

In summary, high quality epitaxial SCTO/ScAlN HEMT heterostructures were demonstrated using oxide MBE. A (111)-oriented SCTO film on ScAlN was achieved by the use of a thin TiO_2 buffer layer, which both lowered lattice and chemical mismatch between the perovskite oxide and the wurtzite nitride layers. TEM imaging conducted on the heterostructure revealed a degraded interface between the SCTO and ScAlN layers, a likely consequence of the piranha chemical treatment of the ScAlN layers prior to oxide deposition. The pretreatment steps were scrutinized, leading to the discovery of an improved process using phosphoric acid to prepare the ScAlN. This new process significantly improved both the structural and electrical properties of the heterostructure after STO growth. Electrical degradation of the HEMT 2DEG was minimized, with an increase in electron mobility of ~50% and a similar reduction in sheet resistance valves compared to the samples grown with the piranha treatment. Finally, the modification of the TiO_2 buffer layer was shown to not significantly alter either the structural or the electrical properties of the STO/ScAlN HEMT heterostructure. The research presented here shows that two very different materials can be epitaxially combined and result in a heterostructure that retains good electrical properties. The demonstrated epitaxial SCTO/ScAlN heterostructures present a new materials system with attractive functional properties that can be exploited in the design of future electronic components to support Navy needs for improved RF switching and power electronics technologies.

5. ACKNOWLEDGEMENTS

The author wishes to acknowledge his colleagues for their contributions to this work: Matthew Hardy, Neeraj Nepal, and Scott Katzer for technical assistance with MBE growth; Andrew Lang for TEM imaging; Brian Downey and Vikrant Gokhale for electrical characterization; and Ginger Wheeler and David Meyer for their supervision and Karles Fellowship nominations.

REFERENCES

[1] M. Akiyama, K. Kano, A. Teshigahara, *Appl. Phys. Lett.* 95, 162107 (2009).

[2] S. Fichtner, N. Wolff, N. Lofink, L. Kienle, B. Wagner, *J. Appl. Phys.* 125, 114103 (2019).

[3] M. T. Hardy, B. P. Downey, N. Nepal, D. F. Storm, D. S. Katzer, D. J. Meyer, *Appl. Phys. Lett.* 110, 162104 (2017).

[4] R. Ranjan, D. Pandey, N. P. Lalla, *Phys. Rev. Lett.* 84, 3726 (2000).

[5] N. K. Kalarickal, Z. Feng, A. F. M. Anhar Uddin Bhuiyan, Z. Xia, W. Moore, J. F. McGlone, A. R. Arehart, S. A. Ringel, H. Zhao, S. Rajan, *IEEE Trans. Electron Devices* 68, 29 (2021).

[6] E. N. Jin, A. C. Lang, M. T. Hardy, N. Nepal, D. S. Katzer, D. F. Storm, B. P. Downey, D. J. Meyer, *J. Appl. Phys.* 127, 214104 (2020).

[7] E. N. Jin, B. P. Downey, V. J. Gokhale, J. A. Roussos, M. T. Hardy, T. A. Growden, N. Nepal, D. S. Katzer, J. P. Calame, D. J. Meyer, *APL Mater.* 9, 111101 (2021).

[8] M. T. Hardy, E. N. Jin, N. Nepal, D. S. Katzer, B. P. Downey, V. J. Gokhale, D. F. Storm, D. J. Meyer, *Appl. Phys. Express* 13, 065509 (2020).

[9] N. Nepal, N. Y. Garces, D. J. Meyer, J. K. Hite, M. A. Mastro, C. R. Eddy, Jr., *Appl. Phys. Express* 4, 055802 (2011).

[10] A. Rice, R. Collazo, J. Tweedie, R. Dalmau, S. Mita, J. Xie, Z. Sitar, *J. Appl. Phys.* 108, 043510 (2010).